








Fraternal twins: distinction between PbPc and SnPc by their switching behaviour in a scanning tunnelling microscope

Roman Forker¹, Marco Gruenewald¹, Falko Sojka¹, Julia Peuker¹, Philipp Mueller^{1,2}, Christian Zwick¹, Tobias Huempfer¹, Matthias Meissner^{1,3} and Torsten Fritz¹

¹ Institut für Festkörperphysik, Friedrich-Schiller-Universität Jena, Helmholtzweg 5, 07743 Jena, Germany

² Leibniz-Institut für Photonische Technologien e. V., Albert-Einstein-Straße 9, 07745 Jena, Germany

³ Institute for Molecular Science, Myodaiji, Okazaki, 444-8585, Japan

E-mail: roman.forker@uni-jena.de

Received 26 October 2018, revised 18 December 2018

Accepted for publication 7 January 2019

Published 7 February 2019




CrossMark

Abstract

In this contribution, we compare the optical absorbance behaviour and the structural properties of lead(II)-phthalocyanine (PbPc) and tin(II)-phthalocyanine (SnPc) thin films. To this end, we employ a Ag(1 1 1) substrate terminated with a monolayer of 3,4,9,10-perylene tetracarboxylic dianhydride constituting an internal interface whose main effect is an electronic decoupling of the phthalocyanine adlayer from the metal surface. As deduced from low-energy electron diffraction and scanning tunnelling microscopy (STM) measurements, the epitaxial relations and unit cell compositions of the prevailing PbPc monolayer and multilayer domains are confusingly similar to those of SnPc on PTCDA/Ag(1 1 1). However, SnPc and PbPc can be readily distinguished by their STM-induced switching behaviours: while the former is capable of reversible configurational changes, no effect on the latter could be achieved by us under comparable conditions. This corroborates earlier theoretical predictions and even renders the chemical identification of individual shuttlecock-shaped metal-phthalocyanines feasible.

Keywords: reversible single-molecule switch, organic-organic heteroepitaxy, differential reflectance spectroscopy (DRS)

 Supplementary material for this article is available [online](#)

(Some figures may appear in colour only in the online journal)

1. Introduction

Switchable molecules controlled through external stimuli have attracted considerable attention, motivated amongst others by potential applications in molecular electronics [1–6]. Single molecule selectivity is often achieved by means of a scanning tunnelling microscope (STM) probing individual molecules adsorbed on a conductive surface, where the switching process can be triggered via resonant electron or hole tunnelling [7–12] or via the force exerted by a functionalized STM tip

[13]. Such investigations are therefore also appealing from the point of view of surface scientists, as they may help understand the adsorbate–substrate interaction and the electronic structure at interfaces on the nanoscale. While the switching between different electronic and/or structural configurations is an intriguing phenomenon as such, its capability to distinguish chemically similar molecules has hardly been explored so far.

In this contribution, we compare lead(II)-phthalocyanine (PbPc) and tin(II)-phthalocyanine (SnPc), both grown on top



of a monolayer (ML) of 3,4,9,10-perylene tetracarboxylic dianhydride (PTCDA), thereby forming an organic internal interface. These metal-phthalocyanines (MPcs) are not entirely planar insofar as the central metal atom protrudes from the phthalocyanine ligand, which is why their shapes are often described as shuttlecocks [14]. Hence, for flat-lying molecules on a surface there are two principally feasible adsorption configurations characterized by the metal atom either pointing away from ('up') or towards the surface ('down'), giving rise to a binary character [14–20] and the general possibility to switch between up and down.

In a broader sense, the term 'switching' is also employed in the literature for STM-based manipulations of the in-plane orientation of individual molecules in the absence of up \leftrightarrow down transitions [21–24]. Here we focus on MPcs embedded in densely packed layers in order to reduce the translational and rotational degrees of freedom of individual molecules. Thus, we expect that up \leftrightarrow down switching events are triggered by our external stimulation instead of modified adsorption sites. Furthermore, STM-induced chemical reactions, such as tautomerization [25], hydrogenation [26], metalation [27], demetalation [28], and bond formation with adatoms [29] have been observed in the literature, but are beyond the scope of this study. For an overview on this topic the reader is referred to the literature [14].

It is well known that metal surfaces can severely influence the switching behaviour of adsorbed molecules. For instance, it was shown for SnPc on Ag(111) that an STM is capable of reversibly switching between the up and down configurations for molecules in the second layer, whereas SnPc molecules in direct contact with this metal substrate could only be switched irreversibly from Sn-up to Sn-down [7]. For first-layer SnPc molecules on Cu(111), however, electrically driven switching was not achieved at all owing to a much higher energy barrier [13]. Since we aim at comparing PbPc and SnPc, whose switching behaviours may be differently influenced by a given metal surface, we use a (111)-oriented silver single crystal passivated by a ML of PTCDA, thereby employing an internal interface that decouples the first MPc layer from the metal surface. In fact, the physisorbed MPc molecules essentially behave electronically like isolated monomers as evidenced by means of optical differential reflectance spectroscopy (DRS) and photoelectron spectroscopy (PES) [30–33]. Consequently, we obtain an unobstructed access to the intrinsic switching properties of PbPc and SnPc with a largely preserved single-molecule character even in laterally densely packed MLs, owing to the diminutive lateral interaction of the MPcs.

These considerations enable us to compare our experiments to earlier investigations using density functional theory (DFT) which were carried out for isolated MPc molecules [34]. Confirming these theoretical predictions, we find that the switching behaviours of SnPc and PbPc differ strongly: SnPc undergoes up (u) \rightarrow down (d) switching in the STM at bias voltages of $V_{u \rightarrow d} \leq -1.6$ V and down \rightarrow up switching at $V_{d \rightarrow u} > +2.1$ V, respectively. Thereby, the adsorption configuration of individual SnPc molecules can be controllably reversed. For PbPc, on the other hand, all our attempts

to switch the molecules in either direction failed for bias voltages between -3.1 and $+3.1$ V. While the optical properties of SnPc and PbPc discussed hereafter only differ to a minor extent and the unit cell parameters of the most densely packed ML structures even turn out to be identical within the experimental accuracy, the chemical discrimination is readily achieved by means of STM via their qualitatively distinct switching behaviour.

2. Methods

Ag(111) single crystals were purchased from MaTeck. PTCDA ($C_{24}H_8O_6$, CAS registry No. 128-69-8) was obtained from Sigma-Aldrich with a nominal purity of 97%. SnPc ($C_{32}H_{16}N_8Sn$, CAS registry No. 15304-57-1) was provided by Achim Schöll and Christoph Sauer, Universität Würzburg. PbPc ($C_{32}H_{16}N_8Pb$, CAS registry No. 15187-16-3) was supplied by Toshiaki Munakata and Takashi Yamada, Osaka University. Prior to usage, the raw materials were purified using temperature gradient sublimation [35].

The optical absorbance of SnPc and PbPc dissolved in benzene (obtained from Roth, purity $> 99.5\%$) was measured *ex situ* with a Varian Cary 5000 UV–vis spectrophotometer.

Sample preparation and thin film deposition were carried out in ultrahigh vacuum (UHV, base pressure 10^{-10} mbar). The silver surfaces were repeatedly sputtered with Ar^+ ions ($1\text{--}3 \mu A \text{ cm}^{-2}$, 700 eV, $\pm 45^\circ$, 30 min) and annealed (700 K) in order to obtain large, atomically flat terraces. Molecular films were grown using organic molecular beam epitaxy (OMBE). The purified powders were kept in effusion cells inside the UHV chamber, where they were thoroughly degassed for several hours before the deposition experiments.

The PTCDA ML was obtained by growing a multilayer film on Ag(111) at $T_{Ag} = 300$ K and then thermally desorbing (at $T_{Ag} \approx 550$ K) all layers except the contact layer. In fact, the first ML of PTCDA is chemisorbed on this substrate [36], which explains its remarkable stability and therefore renders it particularly suitable for the experiments presented here. PTCDA is known to form only one commensurate ML structure on Ag(111) characterized by a surface unit cell containing two molecules with their aromatic planes parallel to the surface and with their long molecular axes being almost perpendicular to one another [36, 37].

PbPc and, for comparison, SnPc layers were grown as published elsewhere [32, 38]. SnPc forms several distinct superstructures with different areal densities on the PTCDA/Ag(111) substrate depending on the amount of deposited phthalocyanine molecules. Therefore, in order to avoid ambiguity, the unit used to indicate the nominal phthalocyanine film thickness is a monolayer equivalent (MLE), where 1 MLE refers to the amount of deposited molecules (instead of surface coverage) necessary to obtain the most densely packed first layer on top of the PTCDA/Ag(111) substrate. For consistency, this definition is also employed for PbPc hereafter.

During film growth we applied optical DRS using the setup detailed elsewhere [39, 40]. In short, this *in situ* technique records the signal

$$\text{DRS}(E, d) = \frac{R(E, d) - R(E, 0)}{R(E, 0)}. \quad (1)$$

Here, $R(E, 0)$ denotes the reflectance of the substrate, and $R(E, d)$ is the reflectance of the substrate covered with an adsorbate of nominal thickness d . The substrate in our case is 1 ML of PTCDA on Ag(111), serving as the reference spectrum $R(E, 0)$, with its optical properties published previously [41]. Hence, the adsorbate here is only the MPc film deposited on top. Its dielectric function $\hat{\epsilon} = \epsilon' - i\epsilon''$ is extracted from the raw DRS data (shown in figure S1 (stacks.iop.org/JPhysCM/31/134004/mmedia) in the supplementary material) using a Kramers–Kronig consistent numerical algorithm [40]. For the discussion of the absorption of the MPc adlayer we focus on the imaginary part ϵ'' of this dielectric function, rather than the imaginary part of the complex index of refraction.

A commercial low-temperature STM (JT-STM/AFM from Specs, $T \approx 1.1$ K) was used for real-space imaging of the samples and also for the switching of MPcs. The samples were probed with an electrochemically etched and Ar⁺-sputtered tungsten tip being part of a KolibriSensor from Specs. The tunnelling voltage is given as sample bias V_S , meaning that $V_S < 0$ V refers to the tunnelling of electrons from occupied levels of the sample into the tip.

While SnPc film structures on PTCDA/Ag(111) have been examined previously [32, 38], the PbPc films grown in this work are furthermore structurally characterized using distortion-corrected low-energy electron diffraction (LEED) [42, 43]. For that purpose, we utilized a device (BDL800IR MCP2 with LaB₆ filament) purchased from OCI Vacuum Microengineering. The micro-channel plates (MCPs) amplify the diffracted electron intensities by a factor in the order of 10^6 which means that the primary electron flux can be reduced accordingly. In fact, we have never observed indications for radiation damage even for prolonged exposure of the samples to the electron beam. During LEED measurements the samples were cooled down from 300 K to approximately 20 K to enhance the contrast. Geometrical simulations of LEED patterns were carried out with the help of LEEDLab [44]. This software contains numerical algorithms to identify the spot positions in the distortion-corrected experimental data, and then optimizes the unit cell parameters by a least-squares fitting routine, thereby increasing both the analytic objectivity and the accuracy, as all visible spots enter the fitting procedure. In the process the numerical error of the fitting procedure is determined, given here as the standard deviation (1σ interval).

3. Results

In the first instance we scrutinize the optical and structural properties of PbPc thin films (in comparison to SnPc) on PTCDA/Ag(111), with emphasis on the ML regime. In doing so, we elaborate how meaningfully their respective switching behaviours can be compared, or to what extent the environments may exert dissimilar influences on those.

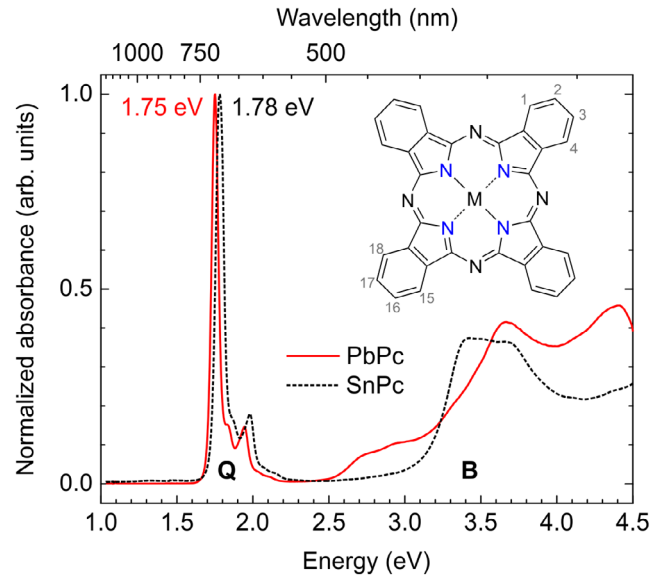


Figure 1. Normalized absorbance spectra recorded at $T = 300$ K for the energetically lowest electronic transitions (Q- and B-bands) of PbPc and SnPc dissolved in benzene. The positions of the peak maxima are indicated. The inset shows the skeletal formula of both MPcs exhibiting C_{4v} symmetry in the ground state [34]. The four isoindole nitrogen atoms coordinating the central metal atom ($M = \text{Pb}, \text{Sn}$) are highlighted in blue. Selected carbon atoms are marked in gray following a conventional numbering scheme [46].

3.1. Optical spectroscopy

3.1.1. Solution spectroscopy. The UV–vis spectra of PbPc and SnPc dissolved in benzene are compared in figure 1. As expected, they exhibit the well-known optical absorbance behaviour of typical MPc monomers whose components were assigned previously [45].

Especially for photon energies below 2.5 eV both spectra are almost identical, the only significant difference being a spectral shift of ≈ 30 meV. Similar shifts of up to ≈ 50 meV depending on the solvent were reported, and in all cases that have come to our knowledge PbPc systematically absorbs at lower energies than SnPc [47, 48]. Thus, the Q-band absorption behaviour might lend itself to discriminate between both molecular species, provided that the spectral resolution is sufficient.

More pronounced differences between PbPc and SnPc arise in the ultraviolet region (B-band, see figure 1) and can be used to distinguish both molecular species more clearly. However, owing to the specific optical properties of silver [49], the spectral region of $E > 3.7$ eV is not well suited for DRS measurements in this case [40].

3.1.2. Differential reflectance spectroscopy. The ϵ'' spectra of PbPc on PTCDA/Ag(111) extracted from the DRS data (figure S1 in the supplementary material) are shown as solid lines in figure 2. Because of the clear overall resemblance to the data of SnPc on PTCDA/Ag(111) published before [38] we discuss the spectral properties only briefly here.

First, we note that the $d_{\text{PbPc}} = 1.0$ MLE curve, albeit somewhat broadened, resembles the absorbance of PbPc in benzene. Thus, the monomeric character of the densely packed

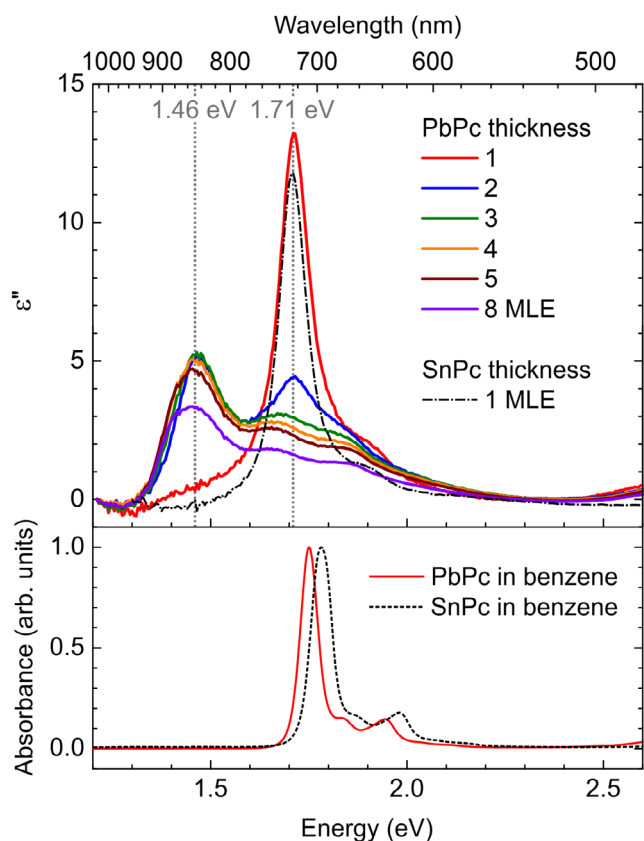


Figure 2. Imaginary part ϵ'' of the dielectric function of PbPc extracted from the DRS data (figure S1 in the supplementary material) recorded at $T = 300$ K, where the substrate is 1 ML of PTCDA on Ag(1 1 1). The corresponding spectrum of 1 MLE of SnPc on the same substrate is depicted to scale for direct comparison [38]. The monomeric character of the 1 MLE spectra of both MPCs on the decoupling PTCDA layer is evidenced by their similarity to the absorbance in solution, shown in the bottom panel (detailed view from figure 1).

PbPc ML on PTCDA/Ag(1 1 1) is essentially preserved, which means that the electronic as well as the optical coupling (i) within the PbPc layer and (ii) between PbPc and the underlying PTCDA/Ag(1 1 1) substrate is rather weak. While PES measurements of PbPc on PTCDA/Ag(1 1 1) have not come to our attention, we expect the electronic interaction across the PbPc/PTCDA interface to be rather weak and predominantly physisorptive based on what is known for similar systems [30–33]. The dash-dotted curve in figure 2 depicts the representative ϵ'' data for 1.0 MLE of SnPc with a pronounced peak maximum of the Q-band at 1.71 eV. The corresponding curve for PbPc differs only slightly, and the peak maxima even coincide to within 5 meV. This contrasts the expectations drawn from the spectral difference between SnPc and PbPc monomers of ≈ 30 –50 meV observed in different solvents as mentioned above. Therefore, the mere peak position of the Q-band maximum is not suitable to readily identify the molecular species in the solid MLs considered here.

Second, from $d_{\text{PbPc}} = 1$ MLE to 2 MLE the ϵ'' spectra undergo a rather abrupt transformation resulting in a new peak at ≈ 1.46 eV, a feature at the position of the initial Q-band maximum (1.71 eV), and a tail at higher photon energies. This

is again closely related to the SnPc data in the same thickness regime (not shown here) and was attributed to the formation of a phthalocyanine bilayer [38]. The occurrence of two main absorption peaks for phthalocyanine dimers can be explained in the framework of an extended dipole model [50] and by means of time-dependent DFT [48]. In fact, the SnPc bilayer was shown to consist of a first layer (adjacent to the PTCDA/Ag(1 1 1) substrate) with Sn-up molecules only, while the second layer (towards the vacuum) exclusively features Sn-down molecules [38]. Owing to the striking similarities between both $d_{\text{MPC}} = 2$ MLE spectra, it is reasonable to assume that the SnPc and PbPc bilayer structures are closely related or even identical, considering the fact that optical spectra, especially those of phthalocyanines, are rather sensitive to the molecular stacking.

Third, above $d_{\text{PbPc}} = 2$ MLE the spectral shape for PbPc multilayers remains fairly unchanged with the exception of the feature at 1.71 eV which apparently diminishes. This differs somewhat from SnPc in the same thickness regime whose low-energy peak continuously shifts from 1.46 eV down in energy, reaching a value of 1.37 eV at $d_{\text{SnPc}} = 12$ MLE, and at the same time reducing in width [38]. While the latter behaviour was attributed to J-type aggregation [51] and a non-negligible interaction between stacked SnPc bilayers, this cannot be equally stated for PbPc. Instead, either the interaction between stacked PbPc bilayers is much less pronounced, or the structural order of PbPc multilayers is inferior to their SnPc counterparts. The latter explanation would also be consistent with the apparent broadening of the PbPc spectra with increasing nominal film thickness.

In summary, for $d_{\text{MPC}} > 2$ MLE there are minor spectral differences between PbPc and SnPc, whereas below this value the prevalent similarities are worth noting.

3.2. Structural characterization

3.2.1. Low-energy electron diffraction. In order to elucidate the long-range order and the unit cell parameters of the heteroepitaxial films, we performed LEED experiments as a function of nominal film thickness subsequent to the deposition, see figures 3 and S2 in the supplementary material.

Except for the PbPc multilayers, all LEED images contain spots belonging to the PTCDA wetting layer on Ag(1 1 1). If the surface unit cell of Ag(1 1 1) is described by two basis vectors with a length of 2.889 Å [52] and a unit cell angle of 120°, then the epitaxy matrix of the commensurate PTCDA ML is $\begin{pmatrix} 3 & 5 \\ -6 & 1 \end{pmatrix}$ [37]. The corresponding reciprocal lattice is depicted in red in figure 3(a). The PTCDA spots maintained their positions irrespective of the PbPc coverage, meaning that the PTCDA/Ag(1 1 1) structure did not change laterally upon PbPc deposition. We note that in similar experiments using copper(II)-phthalocyanine (CuPc, CAS registry No. 147-14-8) the vertical bonding distance between PTCDA and Ag(1 1 1) did change slightly upon CuPc deposition [33]. However, there the lateral PTCDA/Ag(1 1 1) unit cell also remained constant with CuPc adlayers of increasing coverage.

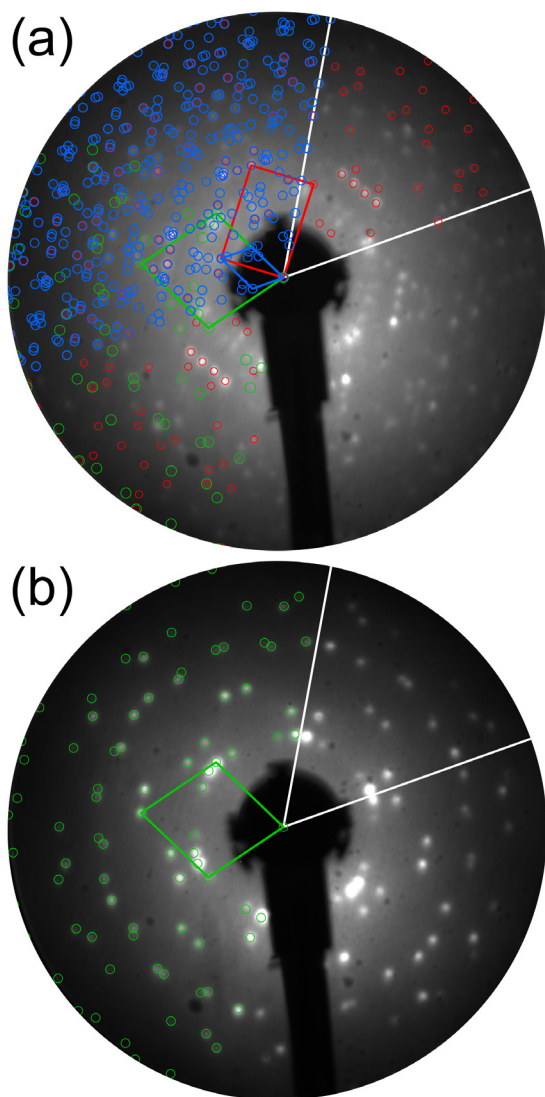


Figure 3. Distortion-corrected LEED images ($E = 23.5$ eV, $T = 20$ K) of PbPc deposited on 1 ML of PTCDA on Ag(111) for (a) $d_{\text{PbPc}} \approx 1.1$ MLE and (b) $d_{\text{PbPc}} \approx 6$ MLE. Different segments of each image are superimposed with geometrical simulations of the LEED patterns containing the Ag(111) single crystal (white lines), the PTCDA wetting layer (red), the PbPc ML phase C (blue), and the PbPc multilayer phase E (green). In all cases the symmetrically equivalent rotational and mirror domains are taken into account, thereby explaining all observed spots. Note that (a) contains spots of phase E which is found from the second PbPc layer onwards.

Therefore, it is likely that also PbPc adsorbates may change the bonding distance between PTCDA and Ag(111) which was not measured in our case, though.

We now turn to a quantitative analysis of the PbPc LEED patterns with the help of LEEDLab. For this purpose, all discernible spots were automatically located, and the reflexes attributable to PTCDA/Ag(111) were excluded from the simulation of the PbPc adlayers. Thereby, we ascertain that if coincidences between PbPc and PTCDA spots exist, then they were not introduced by the LEED simulation performed by us. Table 1 summarizes the structural parameters of all PbPc phases we observed on the PTCDA/Ag(111) substrate. The last column of table 1 indicates refined epitaxy matrices. The

matrices were refined by projecting the PbPc lattice points onto one PTCDA unit cell in real space according to a previously proposed method [53]. For phases A and C one can find fully integer matrices within the numerical uncertainty, hence these phases are commensurate.

Interestingly, the unit cell parameters of the PbPc phases A, C, and E are indistinguishable (within the experimental uncertainty) from the SnPc phases at similar nominal thicknesses and sample temperatures reported earlier [32, 38]. It is also important to note that the PbPc ML phase C, on which switching experiments were performed (see section 3.3), is commensurate [53], which means that there is only a small number of symmetrically inequivalent molecules. Consequently, the physical properties, in particular the switching behaviour of the molecules in one surface unit cell of a commensurate phase, are representative for the entire domain due to translational symmetry.

The PbPc phases B and D were found to occur less frequently. The corresponding LEED images and simulations are presented in figure S2 in the supplementary material. We assume that such minority phases might be a result of slightly varying deposition rates or of site-specific conditions for island formation due to a non-uniform substrate surface, as imposed by substrate steps or other surface defects. We emphasize that a pronounced polymorphism is not uncommon for organic adsorbates, especially for phthalocyanines [14, 16, 54–60]. It is further important to note that for the PbPc phases B and D no SnPc analogue has been reported to date [32, 38]. Since we aim at a comparison of the switching behaviour of both MPcs, phase C of PbPc is particularly important and will thus be characterized in more detail by means of STM in the next section.

3.2.2. Scanning tunnelling microscopy. The most densely packed ML structure C as well as the bilayer of PbPc were further analysed in real space using STM. Figure 4(a) shows a typical STM scan of ≈ 1.1 MLE of PbPc on PTCDA/Ag(111) containing a large ML domain (phase C) and a bilayer island (phase E, as determined from the domain angle θ). This corresponds to the phases observed in the LEED image of figure 3(a). We emphasize that for $d_{\text{PbPc}} \geq 1.0$ MLE the vast majority of the PbPc ML was found to adopt phase C. As soon as bilayer and multilayer domains emerged, their prevailing structural motif was phase E, see table 1.

A close-up view on the ML domain reveals the molecular arrangement, see figure 4(b). The surface unit cell highlighted in blue comprises six PbPc molecules, four of which are Pb-up and the other two are Pb-down. The very same packing motif was observed for 1.0 MLE SnPc on the same PTCDA/Ag(111) substrate. In fact, both MPc/PTCDA heterostructures on Ag(111) are indistinguishable within the uncertainty of our LEED and STM data. This remarkable similarity is consistent with the almost identical lateral dimensions of PbPc and SnPc. DFT-calculations for the free molecules yield a C(2)–C(16) distance (see figure 1 for atom numbering) of 13.048 Å for PbPc and 13.067 Å for SnPc, which agrees to within 0.15% [48]. Contrarily, somewhat different vertical geometries were reported: the distance between the metal

Table 1. Structural parameters of PbPc deposited on 1 ML of PTCDA on Ag(111) as determined via LEED, see figures 3 and S2 in the supplementary material. The epitaxy matrices refer to the PTCDA surface unit cell, characterized by the basis vectors s_1 and s_2 as well as the unit cell angle $\Gamma_{\text{PTCDA}} = \angle(s_2, s_1) = 89.0^\circ$. The basis vectors of the primitive surface unit cell of PbPc are denoted as c_1 and c_2 , the unit cell angle is $\Gamma = \angle(c_2, c_1)$. The domain angle is defined as $\theta = \angle(c_1, s_1)$. For the epitaxy matrices, given in relation to the PTCDA reference lattice being itself commensurate to the Ag(111) substrate, the values in parentheses indicate the numerical errors of the last significant digits as determined by the fitting procedure (scaling error not given here). For the lattice constants c_1 and c_2 the uncertainty of the absolute scaling is also accounted for. The values of d_{PbPc} indicate the nominal thicknesses of PbPc in the analysed LEED images. The last column indicates refined epitaxy matrices according to a method proposed previously [53], see the text for details.

Phase	$d_{\text{PbPc}}/\text{MLE}$	$\ c_1\ /\text{\AA}$	$\ c_2\ /\text{\AA}$	Γ/deg	θ/deg	Epitaxy matrix	Refined epitaxy matrix
A	0.5	25.2(3)	19.0(2)	89.0(2)	0.0(1)	$\begin{pmatrix} 2.004(5) & 0.001(2) \\ 0.000(4) & 1.002(2) \end{pmatrix}$	$\begin{pmatrix} 2 & 0 \\ 0 & 1 \end{pmatrix}$
B	≈ 1.0	14.2(1)	15.2(1)	110.0(2)	49.5(1)	$\begin{pmatrix} 0.715(2) & 0.569(2) \\ -1.140(2) & 0.281(2) \end{pmatrix}$	$\begin{pmatrix} 5/7 & 4/7 \\ -8/7 & 2/7 \end{pmatrix}^{\text{a,b}}$
C	1.1	31.7(5)	41.9(6)	116.6(2)	36.5(1)	$\begin{pmatrix} 2.000(5) & 0.998(3) \\ -2.996(7) & 1.000(4) \end{pmatrix}$	$\begin{pmatrix} 2 & 1 \\ -3 & 1 \end{pmatrix}$
D	1.8	14.0(2)	13.4(2)	101.0(2)	73.8(1)	$\begin{pmatrix} 0.291(3) & 0.708(2) \\ -1.061(2) & 0.064(2) \end{pmatrix}$	$\begin{pmatrix} 5/17 & 12/17 \\ -18/17 & 1/17 \end{pmatrix}^{\text{a,c}}$
E	1.1, 1.8, 6	13.6(2)	14.0(2)	102.3(2)	50.8(1)	$\begin{pmatrix} 0.668(2) & 0.557(2) \\ -1.003(2) & 0.335(1) \end{pmatrix}$	$\begin{pmatrix} 2/3 & 5/9 \\ -1 & 1/3 \end{pmatrix}^{\text{a,d}}$

^a Note that the smallest supercell of a higher order commensurate registry would be oriented differently with respect to the substrate than the primitive unit cell.

^b Smallest supercell of a higher order commensurate registry: $\begin{pmatrix} 1 & -2 \\ 2 & 3 \end{pmatrix} \cdot \begin{pmatrix} 5/7 & 4/7 \\ -8/7 & 2/7 \end{pmatrix} = \begin{pmatrix} 3 & 0 \\ -2 & 2 \end{pmatrix}$.

^c Smallest supercell of a higher order commensurate registry: $\begin{pmatrix} -4 & -3 \\ 3 & -2 \end{pmatrix} \cdot \begin{pmatrix} 5/17 & 12/17 \\ -18/17 & 1/17 \end{pmatrix} = \begin{pmatrix} 2 & -3 \\ 3 & 2 \end{pmatrix}$.

^d Smallest supercell of a higher order commensurate registry: $\begin{pmatrix} 0 & -3 \\ 3 & 1 \end{pmatrix} \cdot \begin{pmatrix} 2/3 & 5/9 \\ -1 & 1/3 \end{pmatrix} = \begin{pmatrix} 3 & -1 \\ 1 & 2 \end{pmatrix}$.

atom and the centre of gravity of the four isoindole nitrogen atoms combined (blue labels in figure 1) is 1.260 Å for PbPc and 1.133 Å for SnPc [34]. This more pronounced shuttlecock shape of PbPc apparently has little influence on the thin film structures formed on PTCDA/Ag(111).

We note that this out-of-plane distance of ≈ 1.2 Å is almost as long as a typical C = C bonding distance (≈ 1.4 Å [34]) and therefore quite substantial, especially in the view of the strong dependence of the tunnelling current on the tip-to-sample distance. Having in mind the delocalized molecular orbitals [7, 34], this rather pronounced geometric effect should be predominant in comparison to possible electronic effects for the contrast of our STM images. It is thus reasonable to conclude that the Pb-up (or Sn-up) molecules are imaged with a bright centre, while Pb-down (or Sn-down) molecules are imaged with a dark centre. In this regard we follow the prevailing interpretation of STM images of such shuttlecock-shaped MPc in the literature [7–13, 15].

Further, an STM scan of a PbPc bilayer is presented in figure 4(c). It is characterized by a surface lattice consistent with phase E in the LEED images in figure 3. Since the orientation of this Ag(111) single crystal is known from previous measurements (the dotted arrow indicates the $[1\bar{1}0]$ -direction) we can assign figure 4(c) to a PbPc bilayer island adsorbed on a rotated and mirrored PTCDA domain. The uppermost PbPc layer contains one Pb-down molecule per surface unit cell. By comparison with SnPc bilayers on the same substrate [38]

it is likely that also the PbPc bilayer is a stack consisting of one Pb-up and one Pb-down layer on PTCDA/Ag(111), and that the optical absorbance behaviour of multilayers is mainly determined by the interaction within such a bilayer. Hence, the similarity of the $d_{\text{MPc}} = 2$ MLE spectra discussed in section 3.1.2 is a result of the chemical *and* structural resemblance between SnPc and PbPc samples. On closer inspection, the height profile of the molecules imaged in figure 4(c) appears not entirely parallel to the surface. However, it is difficult to extract precise topographic information from such images, owing to the well-known convolution with the local density of states present in STM. In a known triclinic bulk crystal phase of PbPc [61] one can find a crystallographic plane (namely the (010)-plane) with lattice dimensions similar to those of phase E. With respect to that particular bulk crystal plane the molecular frameworks are inclined, which by comparison renders the possibility of inclined molecules in phase E plausible. Hence, denoting the adsorbed molecules Pb-up or Pb-down does not necessarily imply molecular planes being exactly parallel to the surface.

3.3. Switching in STM

Motivated by previous reports [7–13, 34] we studied the possibility to switch individual MPc molecules on the decoupled PTCDA ML, using an electrical stimulus in STM. Since we are interested in up \leftrightarrow down switching events, we focus on

MPcs embedded in densely packed layers ($d_{\text{MPc}} = 1.0$ MLE) to reduce the translational and rotational degrees of freedom of individual molecules. In this section, we examine the conditions necessary to switch individual molecules. For that purpose, the following procedure was used: (1) scanning a small area of the sample, (2) placing the STM tip at a selected position, (3) switching off the feedback loop, (4) sweeping the voltage, and (5) scanning the same area again with the feedback loop switched back on. Based on that procedure, we were able to switch SnPc molecules from up to down and vice versa.

3.3.1. Sn-up \rightarrow Sn-down switching. Figure 5 depicts a typical up \rightarrow down switching process of a single SnPc molecule in between two consecutive STM scans. The I–V curves shown there were recorded by sweeping the tip bias from positive to negative (forward sweep, black curve) and then back to positive sample voltage (backward sweep, red curve) as indicated by the dotted arrows. The disparate curve progression hints at a modification of the sample during the measurement. Especially the sudden change of the current in the forward sweep at about -1.8 V can be interpreted as an up \rightarrow down switching. In fact, the much lower current observed after this event is consistent with a movement of the Sn-ion towards the substrate, bearing in mind that the feedback loop was open during I–V measurements and that the tunnelling current depends strongly on the width of the tunnel barrier. The same area was imaged with the STM immediately after recording the I–V curves. The molecule underneath the tip had indeed changed its configuration from Sn-up to Sn-down, as can be inferred from the now missing bright protrusion in its centre.

A few peculiarities occurred during the attempts to switch the molecules. (i) It was not necessary to sweep the voltages—appropriate voltage pulses (typically 50 ms at a bias exceeding the threshold) also led to the desired switching. (ii) Not all molecules could be switched on the first attempt. (iii) Repeated switching attempts may lead to local defect formation, i.e. inclined and sometimes even expelled SnPc molecules. It was possible to level out the inclined molecules (thereby ‘repairing’ the defect) by applying appropriate voltage pulses, or just coincidentally. (iv) The switching of a molecule was influenced to a certain extent by its environment, i.e. dependent on the configuration of neighbouring SnPc molecules. (v) The switching was not always restricted to a specific molecule: sometimes proxy molecules would inadvertently switch instead of the targeted molecule, sometimes two molecules would switch at once. Therefore, the threshold voltages given in this work refer to events where only the targeted molecule underneath the tip had switched without defect formation. More details are described in the supplementary material, figures S3–S5.

In passing we note that Wang *et al* used a slightly different approach to switch SnPc in the STM [7]. Instead of sweeping the voltage (step (4) in our procedure) they recorded a time trace of the tunnelling current $I(t)$ at a fixed negative voltage, and from a sudden drop of the current they inferred

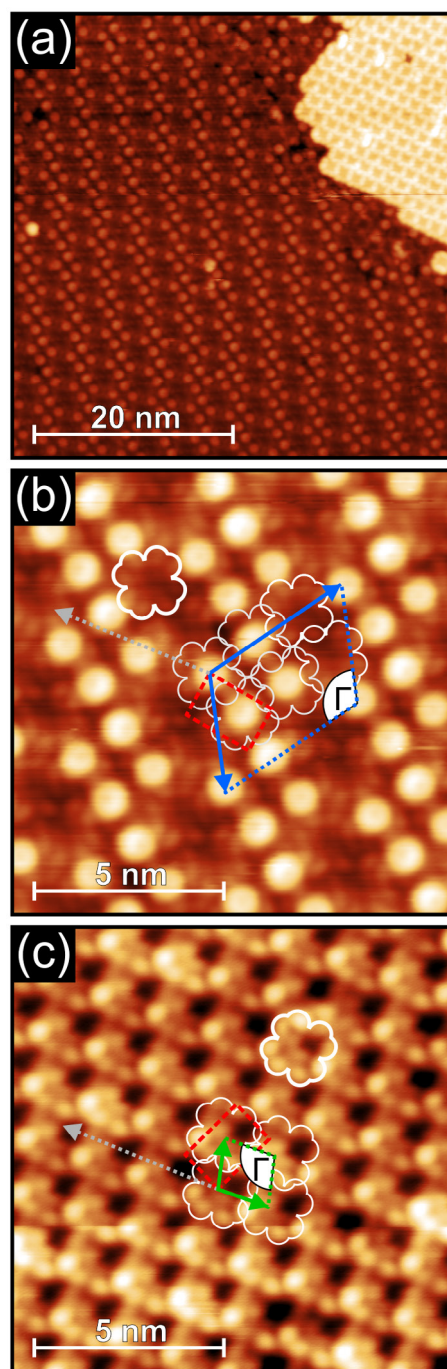


Figure 4. STM images ($V_S = +2.1$ V, $I_{\text{SP}} = 10$ pA, $T = 1.1$ K) of PbPc deposited on 1 ML of PTCDA on Ag(111). (a) Survey scan ($d_{\text{PbPc}} \approx 1.1$ MLE) containing the ML phase C and a bilayer island in the upper right corner. (b) and (c) Close-up views with proposed unit structures. Red dashed lines indicate the respective PTCDA unit cell underneath. Dotted arrows point in the $[1\bar{1}0]$ -direction of Ag (parallel to \vec{s}_1). (b) Phase C with unit cell vectors of the PbPc adlayer indicated in blue. The basis consists of six molecules (visualized by white outlines), four of which are Pb-up featuring a bright protrusion in the molecular centre, and the other two are Pb-down. (c) PbPc bilayer exhibiting phase E, only the upper layer is imaged. All molecules of the upper layer are oriented Pb-down (visualized by white outlines). The unit cell vectors are indicated in green.

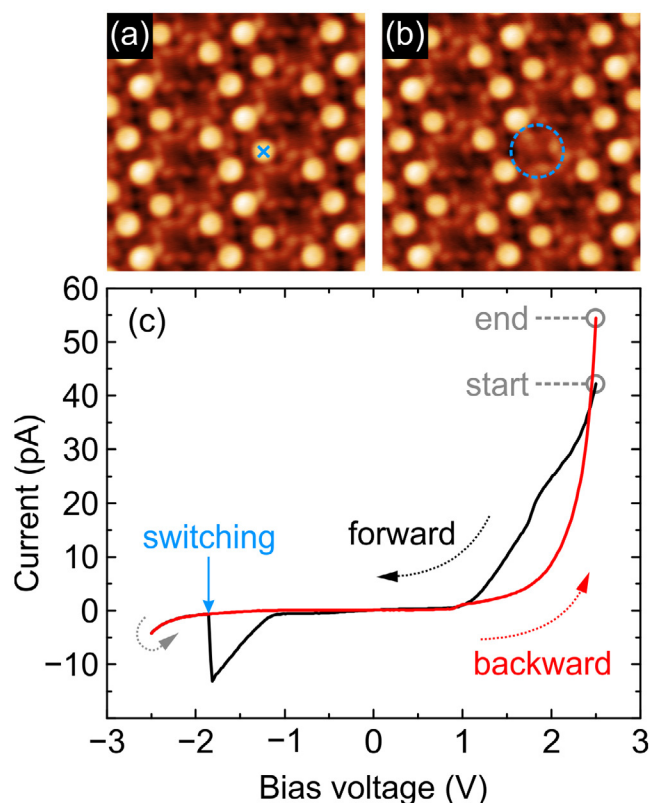


Figure 5. (a) and (b) STM images ($8 \times 8 \text{ nm}^2$, $V_S = +1.5 \text{ V}$, $I_{SP} = 20 \text{ pA}$, $T = 1.1 \text{ K}$) of SnPc ($d_{\text{SnPc}} = 1.0 \text{ MLE}$, structure P1 as determined previously [32]) on 1 ML of PTCDA on Ag(111). After recording frame (a) the tip was placed at the position marked by the cross, and the I-V curves displayed in (c) were recorded by sweeping the voltage in the direction indicated by the dotted arrows. At $V_{u \rightarrow d} \approx -1.8 \text{ V}$ the current exhibits a sudden drop in the forward sweep (black curve), hinting at an up \rightarrow down switching of the molecule below the tip via hole attachment. In the subsequently captured STM image (b) the encircled molecule was found to be Sn-down, as evidenced by the missing bright protrusion.

that an up \rightarrow down switching event via hole attachment had occurred. This procedure is unequivocal for time traces containing a single switching event, because it can be readily verified by subsequent STM imaging. Wang *et al* also observed bidirectional up \leftrightarrow down switching at positive voltages for second-layer SnPc, i.e. molecules on top of a SnPc buffer layer on Ag(111) [7]. There, the rate of these events was shown to depend rather strongly on the applied bias, and the corresponding time traces of the tunnelling current evidently contained several switching events in either direction. However, we refrained from adopting this procedure to our samples in the view of the peculiarities mentioned above. The undesired formation of defects and their possible subsequent ‘repair’ as well as the (possibly also bidirectional) switching of proxy molecules might not be distinguishable from the switching of the targeted molecule underneath the tip. This is especially problematic if the $I(t)$ trace were to exhibit several abrupt changes, so that the subsequently recorded STM image would not allow for an unambiguous assignment of each event in retrospect.

3.3.2. Sn-down \rightarrow Sn-up switching. We found the conditions necessary to stimulate down \rightarrow up switching of SnPc on PTCDA/Ag(111) to be much less reproducible than for the up \rightarrow down process. For example, despite successful up \rightarrow down switching the preceding I-V curves in most cases had no systematic feature (see figure S6 in the supplementary material), in contrast to the prominent kink visible in figure 5. Instead, they were rather noisy, especially at higher voltages of $|V_S| > 2.5 \text{ V}$, which we attribute to instabilities of the tunnelling junction for strong electric fields. This ultimately limits the accessible voltage range for the switching, since instabilities lead to an increased likelihood of local sample damage (e.g. inclined SnPc) or of sudden changes of the tip shape (e.g. by picking up SnPc).

Therefore, we can only roughly determine the threshold for down \rightarrow up switching to be $V_{d \rightarrow u} > +2.1 \text{ V}$ from the applied voltage pulses rather than from I-V measurements. This conservative estimation takes into account the fact that structure P1 of SnPc ($d_{\text{SnPc}} = 1.0 \text{ MLE}$) on PTCDA/Ag(111) can be imaged for prolonged periods at $V_S = +2.1 \text{ V}$ (see figure 6) or even at $V_S = +2.3 \text{ V}$ [32] with extraordinary stability, i.e. without any sign of configurational changes. In comparison to the up \rightarrow down switching (with a lower threshold of $V_{u \rightarrow d} \leq -1.6 \text{ V}$) we observed the tendency that down \rightarrow up switching is characterized by a somewhat higher energy barrier. Quite often it was even necessary to apply $+2.5 \text{ V}$ or higher biases to switch SnPc, which made the molecules in the tunnelling junction more prone to defect formation. Nevertheless, we note that different energy barriers for down \rightarrow up *versus* up \rightarrow down switching are reasonable, given that the underlying substrate imposes an attractive force on the adsorbate and is thus likely to cause an asymmetry in the switching behaviour of Sn-up and Sn-down molecules.

Moreover, the position of the tip is an important parameter. A tip placed above the molecular centre increased our up \rightarrow down switching success rate. This was already reported for first-layer and second-layer SnPc on Ag(111) and explained by a hole attached to the second-to-highest occupied molecular orbital (HOMO-1) which is located mostly in the proximity of the central metal atom [7]. In contrast, tips placed slightly off-centre above an isoindole unit made down \rightarrow up switching in our experiments more successful. Again, for second-layer SnPc on Ag(111) this was attributed to an electron transfer into the second-to-lowest unoccupied molecular orbital (LUMO+1) which extends further onto the phthalocyanine ligand [7].

In order to demonstrate the reversibility of the switching process, figure 6 depicts a sequence of STM scans with deliberate switching of individual SnPc molecules.

3.3.3. Comparison of SnPc and PbPc. Our attempts to switch PbPc molecules in either direction failed for all conditions tested, i.e. at bias voltages between -3.1 and $+3.1 \text{ V}$ and a large variety of tip positions. Therefore, the switching behaviour of SnPc differs substantially from that of PbPc.

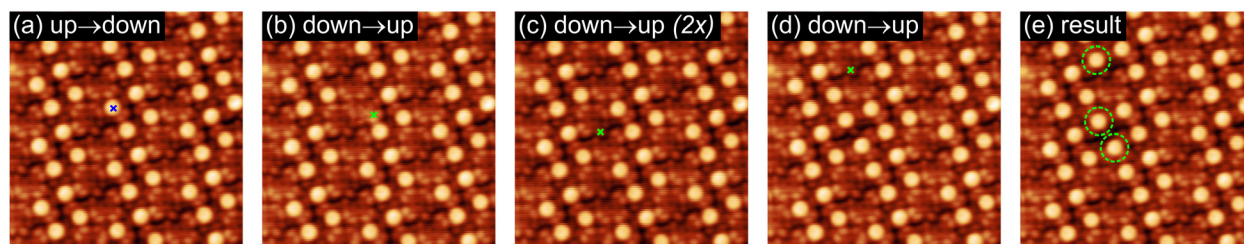


Figure 6. Sequence of STM scans ($10 \times 10 \text{ nm}^2$, $V_S = +2.1 \text{ V}$, $I_{SP} = 10 \text{ pA}$, $T = 1.1 \text{ K}$) of SnPc ($d_{\text{SnPc}} = 1.0 \text{ MLE}$, structure P1 as determined previously [32]) on 1 ML PTCDA/Ag(111). After images (a)–(d) the voltage was swept from $+3.0$ to -3.0 V and back with the tip placed individually above the positions marked by the respective crosses. Between frames (a) and (b) an up \rightarrow down switching of the targeted SnPc occurred (the tip had been above the molecular centre). Between frames (b) and (c) a down \rightarrow up transition of the same molecule took place (the tip had been above an isoindole unit), thereby demonstrating the reversibility of the switching. After frame (c) the targeted molecule and, unintentionally, also its nearest neighbour switched from Sn-down to Sn-up. After another down \rightarrow up switching (d) the resulting pattern (e) exhibited three more Sn-up molecules than frame (a), which are marked by dashed circles.

In a previous report PbPc molecules on MoS_2 apparently changed their configuration upon pulsing (up to $\pm 2 \text{ V}$ for 1 s) as inferred from the dark molecular centres turning bright in subsequent STM frames [62]. However, those experiments were carried out in a nitrogen atmosphere, and the configurational changes were not specific to a particular molecule. Attempts to manipulate individual molecules with the STM (up to $\pm 2 \text{ V}$ for 1 ms) were unsuccessful, and biases higher than $\pm 2 \text{ V}$ even led to the destruction of the PbPc layers [62]. Consequently, although STM-induced configurational changes are not impossible *per se*, no successful switching of individual PbPc molecules have been reported yet, to the best of our knowledge.

In 2010, Baran and Larsson examined shuttlecock-shaped free MPc molecules by means of DFT calculations in detail [34]. They concluded that the transition mechanism of the central metal ion through the phthalocyanine macrocycle is qualitatively different for SnPc and PbPc (both exhibiting C_{4v} symmetry in the ground state): For inversion, SnPc needs to go through two transition states (also of C_{4v} symmetry) with an intermediate local minimum in which the molecule adopts a planar D_{4h} form. This is accompanied by a reversible change of the oxidation state $\text{Sn}^{\text{II}} \rightarrow \text{Sn}^{\text{IV}} \rightarrow \text{Sn}^{\text{II}}$ through intersystem crossing. The energy barrier for this process, i.e. the energetic difference between ground and transition states, was calculated as 3.16 eV . By contrast, the inversion of PbPc involves only one transition state of C_{2h} symmetry in which the central cavity is enlarged due to sizable twisting of the isoindole units on opposite sides. The transition of the Pb ion through the Pc macrocycle requires to overcome a notably higher energy barrier of 4.27 eV . Changing the oxidation state according to $\text{Pb}^{\text{II}} \rightarrow \text{Pb}^{\text{IV}} \rightarrow \text{Pb}^{\text{II}}$ was found to be energetically even less favourable than a distortion of the Pc macrocycle, as opposed to the SnPc case.

Our experiments now support these theoretical predictions, since all our data suggest a considerably lower energy barrier for the switching of SnPc as compared to PbPc in identical environments. Moreover, the voltages of $V_{u \rightarrow d} \leq -1.6 \text{ V}$ necessary to induce up \rightarrow down switching of SnPc on PTCDA/Ag(111) are of slightly smaller magnitude than the threshold of $V_{u \rightarrow d} \approx -1.9 \text{ V}$ reported for the up \rightarrow down switching of

SnPc on the Ag(111) surface [7], meaning that the internal PTCDA/Ag(111) interface present in our samples causes a somewhat lowered energy barrier for the switching process. While Baran and Larsson performed their calculations for free MPc molecules in vacuum, they argued that the presence of a surface could decrease the energy barriers considerably [34]. According to them, a further reduction of the energy barrier for the switching of SnPc would be possible via the interaction with the STM tip and the charge carriers resonantly tunnelling into (or from) the molecule, since this may change the oxidation state of Sn and thus facilitate the transition. On the other hand, given that molecular distortions were found to be the energetically favoured inversion mechanism for PbPc [34], we reason that the tunnelling of charge carriers (despite their potential effect on the Pb oxidation state) does not lower the energy barriers sufficiently to render the switching observable for biases between -3.1 and $+3.1 \text{ V}$. In fact, the van der Waals interaction of the MPc molecules with the underlying PTCDA layer are likely to stabilize the phthalocyanine macrocycle and make its distortion (and therefore the inversion of PbPc) even more improbable.








4. Summary and conclusion

In summary, we characterized the optical and structural properties of the heteroepitaxial system PbPc on 1 ML of PTCDA on Ag(111). Apart from the optical absorbance of the PbPc multilayers the resemblance to SnPc films on the same substrate is remarkable. Metaphorically speaking, PbPc and SnPc behave like fraternal twins that can hardly be told apart. Yet, the discrimination between these two MPcs based on their switching behaviour in the STM is straightforward. While it was readily possible to induce up \rightarrow down and down \rightarrow up switching for SnPc with comparatively low threshold voltages of $V_{u \rightarrow d} \leq -1.6 \text{ V}$ and $V_{d \rightarrow u} > +2.1 \text{ V}$, respectively, we have never achieved the switching of PbPc at bias voltages between -3.1 and $+3.1 \text{ V}$. This substantially distinct behaviour is indicative of a qualitatively different transition mechanism of the central metal atom (Pb *versus* Sn) through the phthalocyanine macrocycle. Our experiments thus support earlier theoretical predictions made for these molecules [34].

Acknowledgments

This research was funded by the Deutsche Forschungsgemeinschaft through Grant Numbers FO 770/2-1 and FR 875/16-1. CZ acknowledges funding from the Carl-Zeiss-Stiftung. TH acknowledges funding from the Studienstiftung des deutschen Volkes. We thank Carsten Ronning for providing access to the *ex situ* UV–vis spectrophotometer.

ORCID iDs

Roman Forker  <https://orcid.org/0000-0003-0969-9180>
 Marco Gruenewald  <https://orcid.org/0000-0003-1545-7831>
 Falko Sojka  <https://orcid.org/0000-0001-5379-1756>
 Christian Zwick  <https://orcid.org/0000-0002-4470-6203>
 Tobias Huempfer  <https://orcid.org/0000-0001-8365-5472>
 Matthias Meissner  <https://orcid.org/0000-0001-6281-2184>
 Torsten Fritz  <https://orcid.org/0000-0001-6904-1909>

References

- [1] Gopakumar T G, Müller F and Hietschold M 2006 *J. Phys. Chem. B* **110** 6051
- [2] Wende H et al 2007 *Nat. Mater.* **6** 516
- [3] Wäckerlin C, Chylarecka D, Kleibert A, Müller K, Iacovita C, Noltling F, Jung T A and Ballav N 2010 *Nat. Commun.* **1** 61
- [4] Niu T and Li A 2013 *J. Phys. Chem. Lett.* **4** 4095
- [5] Zhang J L, Zhong J Q, Lin J D, Hu W P, Wu K, Xu G Q, Wee A T S and Chen W 2015 *Chem. Soc. Rev.* **44** 2998
- [6] Cui X, Troadec C, Wee A T S and Huang Y L 2018 *ACS Omega* **3** 3285
- [7] Wang Y, Kröger J, Berndt R and Hofer W A 2009 *J. Am. Chem. Soc.* **131** 3639
- [8] Nacci C, Kanisawa K and Fölsch S 2012 *J. Phys.: Condens. Matter* **24** 394004
- [9] Huang Y L, Lu Y, Niu T C, Huang H, Kera S, Ueno N, Wee A T S and Chen W 2012 *Small* **8** 1423
- [10] Zhang J L, Xu J L, Niu T C, Lu Y H, Liu L and Chen W 2014 *J. Phys. Chem. C* **118** 1712
- [11] Zhang J, Wang Z, Niu T, Li Z and Chen W 2014 *Appl. Phys. Lett.* **104** 113506
- [12] Song H et al 2017 *Phys. Chem. Chem. Phys.* **19** 22401
- [13] Zhang Y, Wang Y, Lü J-T, Brandbyge M and Berndt R 2017 *Angew. Chem., Int. Ed. Engl.* **56** 11769
- [14] Gottfried J M 2015 *Surf. Sci. Rep.* **70** 259
- [15] Lackinger M and Hietschold M 2002 *Surf. Sci.* **520** L619
- [16] Stadler C, Hansen S, Kröger I, Kumpf C and Umbach E 2009 *Nat. Phys.* **5** 153
- [17] Wang Y, Kröger J, Berndt R and Hofer W 2009 *Angew. Chem., Int. Ed. Engl.* **48** 1261
- [18] Wang Y, Kröger J, Berndt R and Tang H 2010 *J. Am. Chem. Soc.* **132** 12546
- [19] Fan H-L, Lei S-L, Huang J and Li Q-X 2010 *Chin. J. Chem. Phys.* **23** 565
- [20] Sperl A, Kröger J and Berndt R 2011 *J. Phys. Chem. A* **115** 6973
- [21] Liu J, Li C, Liu X, Lu Y, Xiang F, Qiao X, Cai Y, Wang Z, Liu S and Wang L 2014 *ACS Nano* **8** 12734
- [22] Li C, Xiang F, Wang Z, Liu X, Jiang D, Wang G, Zhang X, Chen W and Wang L 2014 *Mater. Res. Express* **1** 045101
- [23] Niu T 2015 *J. Phys. Chem. C* **119** 19802
- [24] Li C, Wang Z, Lu Y, Liu X and Wang L 2017 *Nat. Nanotechnol.* **12** 1071
- [25] Liljeroth P, Repp J and Meyer G 2007 *Science* **317** 1203
- [26] Yang K, Liu L, Zhang L, Xiao W, Fei X, Chen H, Du S, Ernst K-H and Gao H-J 2014 *ACS Nano* **8** 2246
- [27] Sperl A, Kröger J and Berndt R 2011 *Angew. Chem., Int. Ed. Engl.* **123** 5406
- [28] Sperl A, Kröger J and Berndt R 2011 *J. Am. Chem. Soc.* **133** 11007
- [29] Mohn F, Repp J, Gross L, Meyer G, Dyer M S and Persson M 2010 *Phys. Rev. Lett.* **105** 266102
- [30] Häming M, Greif M, Wießner M, Schöll A and Reinert F 2010 *Surf. Sci.* **604** 1619
- [31] Häming M, Greif M, Sauer C, Schöll A and Reinert F 2010 *Phys. Rev. B* **82** 235432
- [32] Gruenewald M, Sauer C, Peuker J, Meissner M, Sojka F, Schöll A, Reinert F, Forker R and Fritz T 2015 *Phys. Rev. B* **91** 155432
- [33] Stadtmüller B, Willenbockel M, Schröder S, Kleimann C, Reinisch E M, Ules T, Soubatch S, Ramsey M G, Tautz F S and Kumpf C 2015 *Phys. Rev. B* **91** 155433
- [34] Baran J D and Larsson J A 2010 *Phys. Chem. Chem. Phys.* **12** 6179
- [35] Levin A A, Leisegang T, Forker R, Koch M, Meyer D C and Fritz T 2010 *Cryst. Res. Technol.* **45** 439
- [36] Zou Y, Kilian L, Schöll A, Schmidt T, Fink R and Umbach E 2006 *Surf. Sci.* **600** 1240
- [37] Kilian L, Umbach E and Sokolowski M 2004 *Surf. Sci.* **573** 359
- [38] Gruenewald M, Peuker J, Meissner M, Sojka F, Forker R and Fritz T 2016 *Phys. Rev. B* **93** 115418
- [39] Forker R and Fritz T 2009 *Phys. Chem. Chem. Phys.* **11** 2142
- [40] Forker R, Gruenewald M and Fritz T 2012 *Annu. Rep. Prog. Chem. C* **108** 34
- [41] Gruenewald M, Wachter K, Meissner M, Kozlik M, Forker R and Fritz T 2013 *Org. Electron.* **14** 2177
- [42] Sojka F, Meissner M, Zwick C, Forker R and Fritz T 2013 *Rev. Sci. Instrum.* **84** 015111
- [43] Sojka F, Meissner M, Zwick C, Forker R, Vyshnepolsky M, Klein C, Horn-von Hoegen M and Fritz T 2013 *Ultramicroscopy* **133** 35
- [44] LEEDLab 2018 version 1.0 2018 Falko Sojka and Torsten Fritz, Fritz & Sojka GbR, Apolda, Germany
- [45] de la Torre G, Vázquez P, Agulló-López F and Torres T 2004 *Chem. Rev.* **104** 3723
- [46] Rawling T and McDonagh A 2007 *Coord. Chem. Rev.* **251** 1128
- [47] Sayer P, Gouterman M and Connell C R 1982 *Acc. Chem. Res.* **15** 73
- [48] Sumimoto M, Honda T, Kawashima Y, Hori K and Fujimoto H 2012 *Dalton Trans.* **41** 7141
- [49] Jiang Y, Pillai S and Green M A 2016 *Sci. Rep.* **6** 30605
- [50] Sakakibara Y, Saito K and Tani T 1998 *Japan. J. Appl. Phys.* **37** 695
- [51] Hestand N J and Spano F C 2018 *Chem. Rev.* **118** 7069
- [52] Yang J, Dennis R C and Sardar D K 2011 *Mater. Res. Bull.* **46** 1080
- [53] Forker R, Meissner M and Fritz T 2017 *Soft Matter* **13** 1748
- [54] Wang Y, Ge X, Manzano C, Kröger J, Berndt R, Hofer W A, Tang H and Cerda J 2009 *J. Am. Chem. Soc.* **131** 10400
- [55] Kröger I et al 2010 *New J. Phys.* **12** 083038
- [56] Kröger I, Bayersdorfer P, Stadtmüller B, Kleimann C, Mercurio G, Reinert F and Kumpf C 2012 *Phys. Rev. B* **86** 195412
- [57] Kröger I, Stadtmüller B and Kumpf C 2016 *New J. Phys.* **18** 113022
- [58] Scheffler M, Smykalla L, Baumann D, Schlegel R, Hänke T, Toader M, Büchner B, Hietschold M and Hess C 2013 *Surf. Sci.* **608** 55
- [59] Niu T, Zhang J and Chen W 2014 *J. Phys. Chem. C* **118** 4151
- [60] Kawakita N, Yamada T, Meissner M, Forker R, Fritz T and Munakata T 2017 *Phys. Rev. B* **95** 045419
- [61] Iyechika Y, Yakushi K, Ikemoto I and Kuroda H 1982 *Acta Crystallogr. B* **38** 766
- [62] Strohmaier R, Ludwig C, Petersen J, Gompf B and Eisenmenger W 1996 *J. Vac. Sci. Technol. B* **14** 1079